ROYAL SOCIETY
OF CHEMISTRY

EDGE ARTICLE

Check for updates

Discovery of an allosteric 14-3-3 inhibitor for suppressing NRF2-driven cancer *via* phenotypic screening and chemoproteomic-based target deconvolution

Jinglong Zhao, [ID] [a] Han Jiang, [a] Kaimei Zhao, [a] Tian Liu, [a] Qiong Zhang, [a] Ziquan Zhao, [a] Junjie Wang, [a] Qidong You, [ID] *[ab] Mengchen Lu*[c] and Zhengyu Jiang [ID] *[ab]

The NRF2 transcription factor is constitutively active in various cancers, functioning as an oncogenic driver for tumor progression and chemo/radiotherapy resistance. Despite the well-documented role of NRF2 overactivation in cancer, no targeted therapy is currently available. In this study, using a combination of phenotypic screening, chemoproteomics, and biochemical and cellular assays, we identified WS3 as a potent allosteric inhibitor of 14-3-3 that selectively inhibits NRF2 activity in tumor cells. Mechanistically, WS3 binds allosterically to the 14-3-3 dimer, inducing a conformational change and disrupting the 14-3-3–pGSK3β interaction, thereby releasing pGSK3β for dephosphorylation. This activation of GSK3β subsequently enhances the ubiquitination and degradation of NRF2 by the CUL1−β-TrCP E3 ligase. WS3 effectively elicits oxidative stress and potentiates chemotherapeutics and ferroptosis in NRF2-driven cancers. Our findings uncover a previously unrecognized role of 14-3-3 in the hyperactivation of NRF2 and present a first-in-class sub-micromolar 14-3-3 allosteric inhibitor as an effective therapeutic strategy to suppress NRF2 overactivation, especially in Keap1 defective cancers.

Introduction

Nuclear factor erythroid-2-related factor 2 (NRF2), a Cap'n'collar (CNC) basic leucine zipper (b-Zip) family transcription factor, plays critical roles in regulating redox homeostasis, cellular metabolism and cell survival by regulating numerous cytoprotective genes containing the antioxidant responsive element (ARE) sequence.[1–3] While NRF2 protects healthy cells from oxidative and electrophilic stress, its overactivation in cancer cells can result in oxidative stress resistance, metabolic reprogramming, ferroptosis inhibition and chemotherapy resistance.[4–6] Numerous studies across various cancers have demonstrated that NRF2 inhibition sensitizes cancer cells to anticancer therapies, particularly in Non-Small Cell Lung Cancer (NSCLC), which frequently harbors mutations in the KEAP1 or NFE2L2 genes.[7] Given the dual roles of NRF2 in normal and cancer cells, the approach for NRF2 inhibition should be context-dependent, emphasizing selective inhibition in cancer cells while sparing normal cells to maximize the

therapeutic index. However, to date, only a few NRF2 inhibitors have been reported, with brusatol,[8] ML385,[9] MSU38225 (ref. 10) and R16 (ref. 11) serving as representative compounds. Recently, a Keap1 covalent molecular glue VVD-065, which allosterically promotes Keap1–CUL3 interaction to enhance NRF2 degradation, has advanced to the phase I clinical trials.[12]

NRF2 activity is restricted at the protein level by two principal E3 ubiquitin ligases: the Keap1/Cullin3-mediated complex and the β-TrCP/Cullin1-mediated complex.[13] Under basal conditions, Keap1 binds to NRF2 and directs it towards Cullin3-dependent ubiquitylation and subsequent proteasomal degradation.[14] However, loss of function mutations in KEAP1 or gain of function mutations in NFE2L2 in cancers significantly abrogates the inhibitory function of KEAP1, leading to NRF2 overactivation.[15] Alternatively, β-TrCP–CUL1 mediates NRF2 degradation in a signaling-pathway dependent manner. It recognizes the phosphorylated DSGIS motif in NRF2 and directs it to Cullin1-based ubiquitylation and proteasomal degradation. A previous study demonstrated that the β-TrCP-mediated pathway acts as an auxiliary system when Keap1-mediated degradation is profoundly suppressed.[16,17] However, GSK3β, the primary kinase responsible for NRF2 phosphorylation, is inhibited by the oncogenic AKT signaling pathway *via* phosphorylation at Ser9,[18] thereby suppressing β-TrCP-mediated NRF2 degradation. These results underscore the urgent need

[a] Jiang Su Key Laboratory of Drug Design and Optimization, Department of Medicinal Chemistry, School of Pharmacy, China Pharmaceutical University, Nanjing 210009, China. E-mail: youqd@163.com; jiangzhengyucpu@163.com

[b] State Key Laboratory of Natural Medicines, China Pharmaceutical University, Nanjing 210009, China

[c] Department of Medicinal Chemistry, College of Pharmaceutical Sciences, Soochow University Medical College, Suzhou 215123, China. E-mail: mclu@suda.edu.cn

to develop potent NRF2 inhibitors that employ novel mechanisms of action.

14-3-3 proteins are a family of evolutionarily conserved scaffold proteins comprising seven isoforms (β/α, γ, ε, ζ/δ, η, σ and τ), which predominantly exist as dimers and participate in various physiological processes.[19] These proteins interact with and regulate the function of serine/threonine phosphorylated proteins.[20–22] The impact of 14-3-3 proteins on their interacting partners can vary from inhibition or activation of catalytic activity and sequestration (e.g., out of the nucleus), to the scaffolding of protein–protein interactions, in a context-dependent manner.[23] Emerging evidence has demonstrated that distinct 14-3-3 isoforms are frequently upregulated in specific cancer types, contributing to oncogenic activities including cell growth, cell cycle, apoptosis, migration, and invasion.[24,25] Notably, previous studies identified 14-3-3ζ as a novel prognostic biomarker for NSCLC.[26] Overexpression of 14-3-3ζ enhances the phosphorylation of Akt, promotes the proliferation of NSCLC cell lines, and contributes to chemoresistance. Therefore, directly targeting 14-3-3ζ or the combination of conventional therapeutic approaches with 14-3-3ζ-targeted therapies may hold significant therapeutical potential.

In this work, we elucidate a previously unrecognized function of 14-3-3 proteins in NRF2 hyperactivation and present a first-in-class sub-micromolar 14-3-3 allosteric inhibitor for NRF2 suppression. Through phenotypic screening of our in-house library, we identified compound WS3 as a potent NRF2 inhibitor. Chemoproteomics-based target deconvolution identified 14-3-3 proteins as the primary cellular target of WS3. Mechanistically, WS3 binds allosterically to 14-3-3, inducing conformational changes and altering dimer formation, interrupting the interaction between 14-3-3 and the inactive pGSK3β. Upon dissociation from 14-3-3, the inactive pGSK3β could be dephosphorylated by protein phosphatase 2A (PP2A), converting it into an active form. Active GSK3β subsequently phosphorylates NRF2 at Ser344, facilitating its ubiquitination and degradation by the auxiliary CUL1–β-TrCP E3 ligase. Importantly, WS3 preferentially inhibits NRF2 functions in tumor cells, inducing oxidative stress and sensitizing tumors cells to chemotherapeutics and ferroptosis. Together, our findings provide new avenues for developing potent 14-3-3 allosteric inhibitors and explore the therapeutic potential of targeting 14-3-3 proteins for suppressing NRF2-addicted cancer growth.

Results

Phenotypic screening identifies potent NRF2 inhibitors in tumor cells

To identify small molecules that inhibit NRF2 with unknown mechanisms, we used A549 cells harboring an ARE sequence upstream of luciferase (ARE-LUC) to perform the phenotypic screening of NRF2 inhibitors. We adapted the ARE-responsive reporter assay to a 96-well format and then screened an in-house library of ∼900 compounds for NRF2 inhibition activity (Fig. S1A). More than one hundred compounds were identified that inhibited the NRF2–ARE signal to 60 percent at a concentration of 1 μM (Fig. 1A). Further concentration-response assays

identified 18 compounds with half-maximal inhibition activities below 200 nM. Then, we reconfirmed their inhibition in NRF2 downstream targets HO-1 and GCLM, along with elaborate literature research to exclude compounds with known mechanisms of NRF2 regulation (Table S1). Finally, we identified WS3 (Fig. 1B), which potently inhibited the NRF2–ARE signal (IC$_{50}$ = 135 nM, Fig. 1C). WS3 exhibited concentration and time dependent downregulation of the expression of NRF2 downstream targets HO-1 and GCLM at both mRNA and protein levels in A549 cells as well as other NSCLC cell lines (Fig. 1D and S1B). WS3 treatment also reduced the NRF2 protein level (Fig. 1E). Notably, WS3 hardly affected the NRF2 activity in normal HUVEC and BEAS-2B cells (Fig. 1F). Moreover, WS3-mediated NRF2 downregulation could be partially rescued by the proteasome inhibitor MG132 (Fig. 1G), suggesting the involvement of proteasome/ubiquitin-mediated degradation. Ubiquitination immunoblotting analysis showed that WS3 indeed promoted the ubiquitination of NRF2 (Fig. 1H). There are two primary E3 ligase complexes regulating NRF2 ubiquitination, the Rbx1–CUL3–Keap1 E3 complex and SKP1–CUL1–β-TrCP E3 complex. Given the loss-of-function mutations in KEAP1 in A549 cells,[27] we hypothesized that WS3 might act through the SKP1–CUL1–β-TrCP E3 complex. Knockdown of either component of the SKP1–CUL1–β-TrCP complex impaired WS3 activity (Fig. S1C) and knockdown of other Cullins exhibited no effect on the activity of WS3 (Fig. S2A to E), supporting this hypothesis. Previous study identified WS3 as an activator of β cell proliferation through targeting EBP1.[28] However, knockdown of EBP1 in A549 cells hardly affected WS3 activity (Fig. 1I), suggesting that an unknown target mediates the inhibitory function of WS3 on NRF2.

Discovery and confirmation of the cellular target of WS3

To deconvolute the relevant target of WS3, we synthesized the clickable photo-affinity probe, WS3-PAL for photo-affinity labeling, a typical chemoproteomic method in target identification (Fig. 2A).[29] WS3-PAL retained cellular activity in ARE-LUC reporter assays (IC$_{50}$ = 155 nM) (Fig. 2B) and effectively downregulated the mRNA level of the NRF2 target gene HO-1 (Fig. S3A), confirming its suitability for labeling experiments. Treatment of A549 cells with WS3-PAL, followed by ultraviolet (UV) crosslinking, click-reaction-based conjugation of biotin azide, enrichment with streptavidin and silver staining for visualization, revealed two main bands at ∼28 and ∼100 kDa predominantly labeled by different probe concentrations (Fig. 2C). Liquid chromatography-tandem mass spectrometry analysis of enriched proteins identified several 14-3-3 family proteins with a high enrichment ratio, with 14-3-3ζ ranked the highest (Fig. 2D). These findings suggest that 14-3-3 proteins are potential binding partners of WS3.

We conducted various assays in situ and in vitro to confirm the direct binding of WS3 to 14-3-3. First, WS3-PAL dose-dependently labeled endogenous 14-3-3ζ in A549 cells as well as purified recombinant 14-3-3ζ, which could be competitively offset by the excess of WS3 (Fig. 2E and S3B). Then, ITC analysis indicated that WS3 directly binds to 14-3-3ζ in a 1 : 1 ratio, with
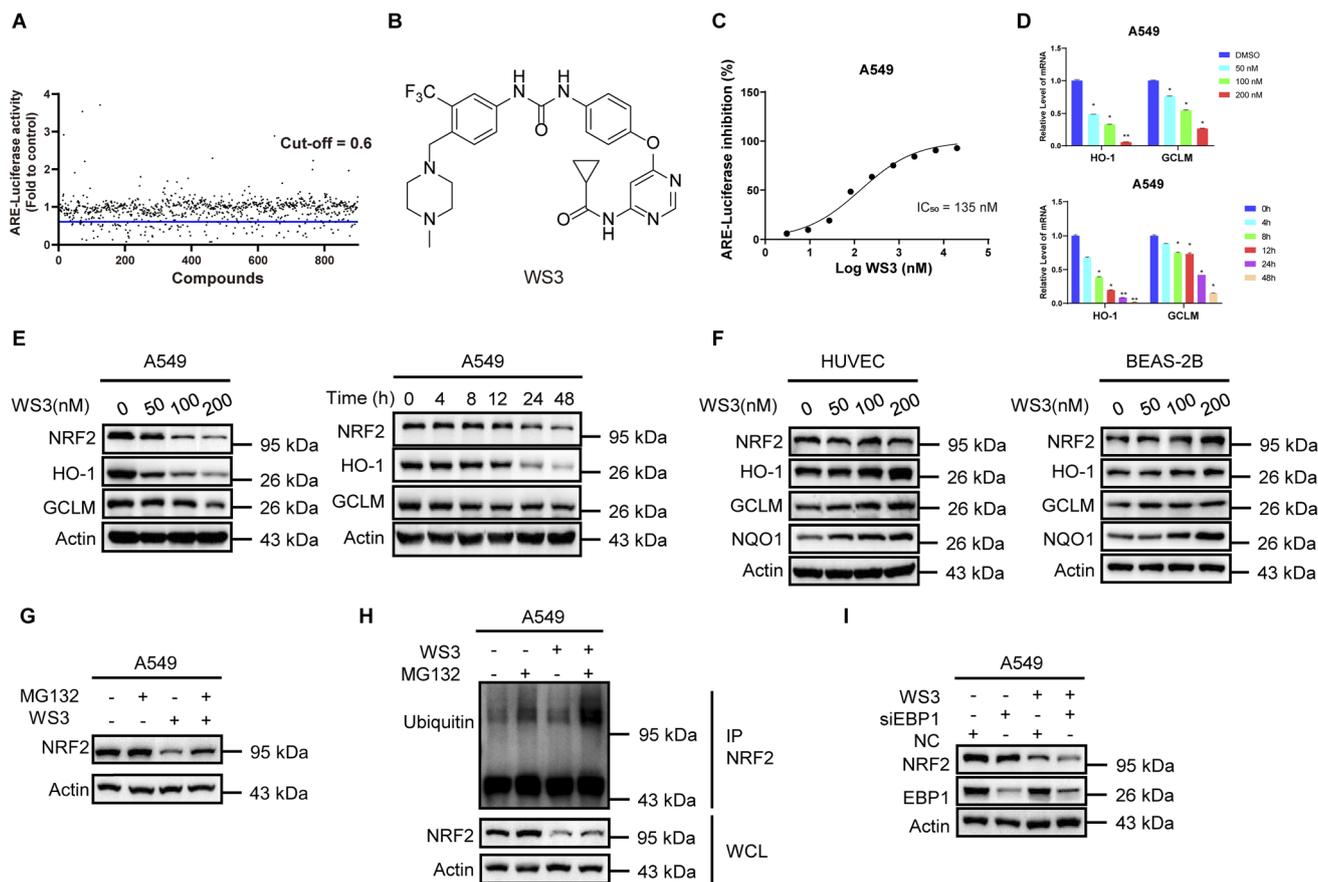
Fig. 1 Phenotypic screening identified small molecule WS3 that inhibits the NRF2 pathway selectively in tumour cells. (A) High-throughput screening of a 900 small-molecule compound library at 1 µM concentration with the A549-ARE reporter cell line. The cut-off value for ARE-luciferase activity is 0.6. (B) Structure of the hit compound WS3. (C) ARE-luciferase reporter activities in A549 cells treated with WS3 for 48 h. Mean and s.e.m. (D) Relative transcript levels of NRF2-target genes (HO-1 and GCLM) in A549 cells treated with WS3 (50, 100, and 200 nM) for 48 h or 100 nM WS3 for different times. Mean and s.e.m. (E) Immunoblot analysis of the protein level of NRF2 and downstream targets (HO-1 and GCLM) in A549 cells treated with WS3 (50, 100, and 200 nM) for 48 h or 100 nM WS3 for different times. (F) Immunoblot analysis of NRF2 and downstream targets (HO-1 and GCLM) in human normal cells (BEAS-2B and HUVEC) treated with WS3 (50, 100, and 200 nM) for 48 h. (G) Immunoblot analysis of NRF2 protein in A549 cells. Cells were pretreated with DMSO or WS3 (200 nM) for 24 h before additional MG132 (10 µM) treatment for 12 h. (H) Immunoblot analysis of NRF2 protein ubiquitination in A549 cells. A549 cells were pretreated with WS3 (10 µM) for 24 h and MG132 (10 µM) as indicated for 12 h before immunoprecipitation (IP) and immunoblotting (IB). (I) Immunoblot analysis of NRF2 protein in A549 cells. Cells were pretreated with the EBP1 siRNA for 24 h before additional WS3 (200 nM) treatment for 48 h. Statistical analyses are univariate two-sided t-tests. *$P < 0.05$. Data are representative of at least 2 biological replicates.

K_d values of 2.29 µM. Meanwhile, ITC revealed that the contribution of entropic ($-T\Delta S$) to the binding is larger than enthalpy (ΔH), and thus the binding appears to be driven by the hydrophobic effect, or a change in the protein secondary structure upon WS3 binding. Furthermore, WS3 also binds to 14-3-3τ and 14-3-3η with high affinities, suggesting that WS3 may be a pan 14-3-3 binder with relatively low selectivity (Fig. 2F and S3C). Bioinformatics analysis confirmed *YWHAZ* (14-3-3ζ) as the most significantly overexpressed isoform in NSCLC patients and A549 cells (Fig. S3D to F), and elevated *YWHAZ* (14-3-3ζ) was positively correlated with poor prognosis and upregulation of oncogenic NRF2 pathways in LUAD patients (Fig. S3G to I). Based on these findings, *YWHAZ* was selected for further studies. The cellular thermal shift assay (CETSA) demonstrated that treatment with WS3 enhanced the 14-3-3ζ thermal stabilization compared to the DMSO control, suggesting the intracellular binding between

WS3 and 14-3-3ζ (Fig. 2G). Furthermore, using WS3-PAL that could be conjugated with a fluorophore *in situ* for live cell imaging assays, we observed obvious colocalization with 14-3-3ζ in A549 cells, with a Person correlation coefficient (R) of about 0.77 ($R > 0.6$, means strong correlation, Fig. S3J). Surface plasmon resonance (SPR) and microscale thermophoretic (MST) assays both confirmed WS3 binding to 14-3-3ζ, with K_d values of 2.3 µM and 3.2 µM respectively (Fig. S3K and L). Nuclear magnetic resonance (NMR) analysis revealed positive saturation transfer difference (STD) signals in the STD spectrum, further validating the binding between WS3 and 14-3-3ζ (Fig. 2H and Table S2). Mapping the relative STD NMR signals onto WS3 indicates that protons H4, H6, H21 and H24 make the closest contacts with the 14-3-3 binding surface, as shown by their larger STD enhancements. In contrast, the piperazine and cyclopropyl groups showed lower STD effects, suggesting that
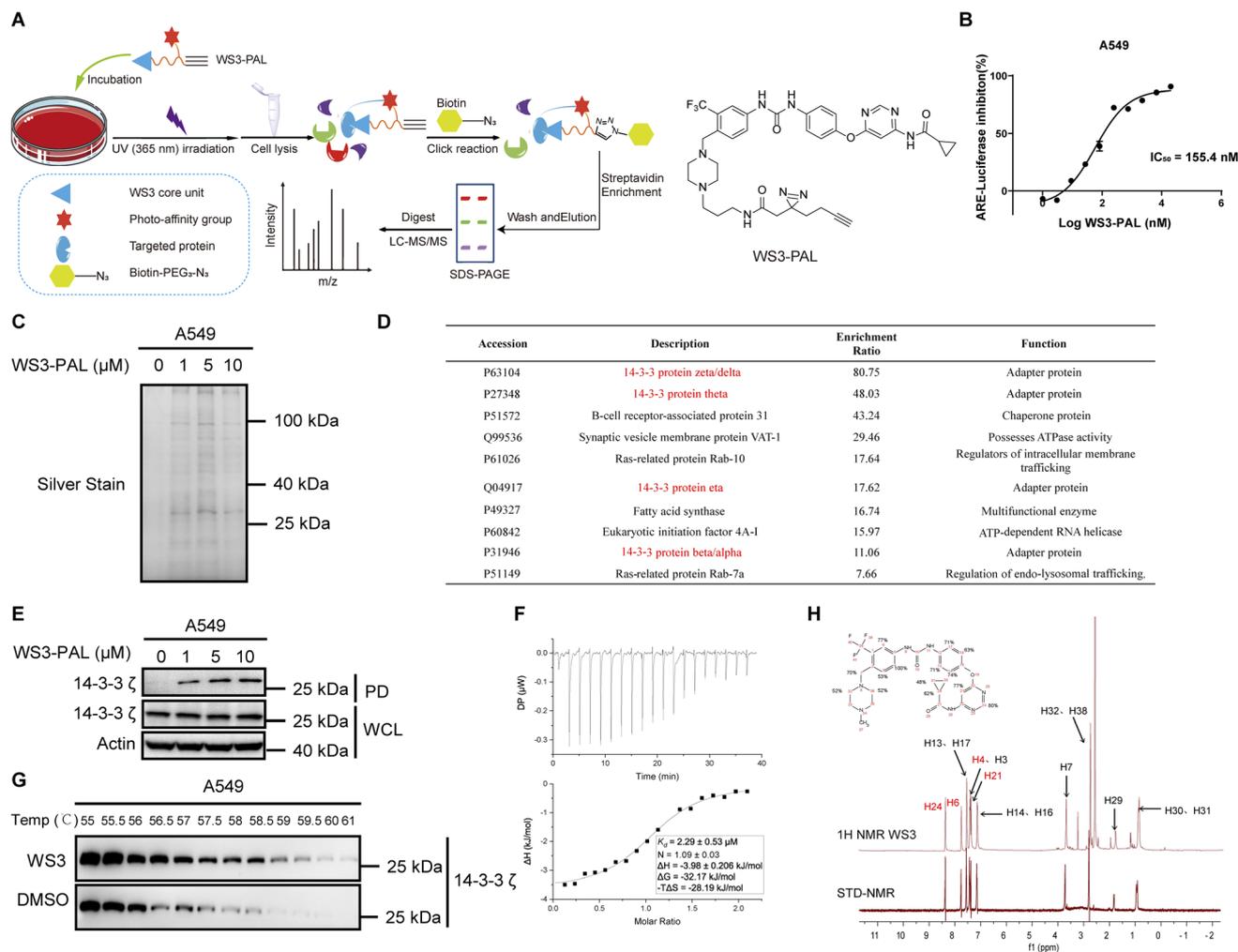
Fig. 2 Discovery and confirmation of the 14-3-3 protein as the primary target of WS3 in A549 cells. (A) Schematic illustration of photoaffinity-labeling based target identification and chemical structure of the photo-activatable affinity probe WS3-PAL. (B) ARE-luciferase reporter activities in A549 cells treated with WS3-PAL for 48 h. Mean and s.e.m. (C) In situ photo-labeling and pull-down of WS3-PAL covalent labeled targets. A549 cells were treated with WS3-PAL (1, 5, and 10 μM) for 4 h, and the total proteins were silver-stained. (D) MS/MS results of the top ten proteins enriched by photoaffinity pulldown experiments ranked based on the enrichment ratio (normalized to the total concentration in A549 cells). (E) Biotin pull-down (PD) followed by western blot with antibody for 14-3-3 validates the labelling of 14-3-3ζ exposed to WS3-PAL in A549 cell lysates. A549 cells were treated with WS3-PAL (1, 5, and 10 μM) for 4 h. (F) Isothermal titration calorimetry (ITC) analysis of the 14-3-3ζ (350 μM, monomer) association with WS3 (30 μM). (G) Cellular thermal shift assay (CETSA) analysis of intracellular binding between WS3 and 14-3-3ζ in A549 cells. Cells were treated with WS3 (10 μM) for 4 h. Western blot signals for 14-3-3ζ and total protein staining of the soluble fraction are shown for each condition. (H) Saturation transfer difference (STD)-NMR analysis of the direct interaction between 14-3-3ζ (10 μM) and WS3 (400 μM). The relative degree of saturation of the individual hydrogens is mapped into the structure and normalized to that of hydrogen H4. Data are representative of at least 2 biological replicates.

they are oriented toward the solvent. Collectively, these results demonstrate that 14-3-3ζ is a direct target of WS3 in A549 cells.

WS3 binds allosterically to 14-3-3 and induces 14-3-3 dimer conformational changes

The 14-3-3 proteins primarily exist as dimers, with each monomer composed of nine antiparallel α-helices (α1–α9) that form an amphipathic groove capable of binding to protein partners.[30] While the binding grooves are highly conserved, the outer surface of the central groove exhibits a high degree of variability.[31] Given that the photo-affinity probe WS3-PAL showed similar NRF2 inhibition activity to WS3 in A549 cells,

and excess WS3 decreased the pulldown of 14-3-3ζ by WS3-PAL for competition, WS3-PAL and WS3 likely occupy the same binding pocket on 14-3-3ζ. To identify the residue(s) responsible for WS3 binding, we incubated the purified 14-3-3ζ protein with WS3-PAL, followed by UV irradiation on ice for covalent crosslinking. The complex was digested with trypsin and subjected to LC-MS/MS analysis. A 718 Da increase in molecular weight, corresponding to the photoactivated WS3-PAL fragment, was detected to bind at E66 of the peptide 74-VVSSIEQKTEGAEK-87 (Fig. 3A and S4A), suggesting that the binding sites lie within the pocket containing this peptide motif. Notably, this motif did not lie in the central orthosteric
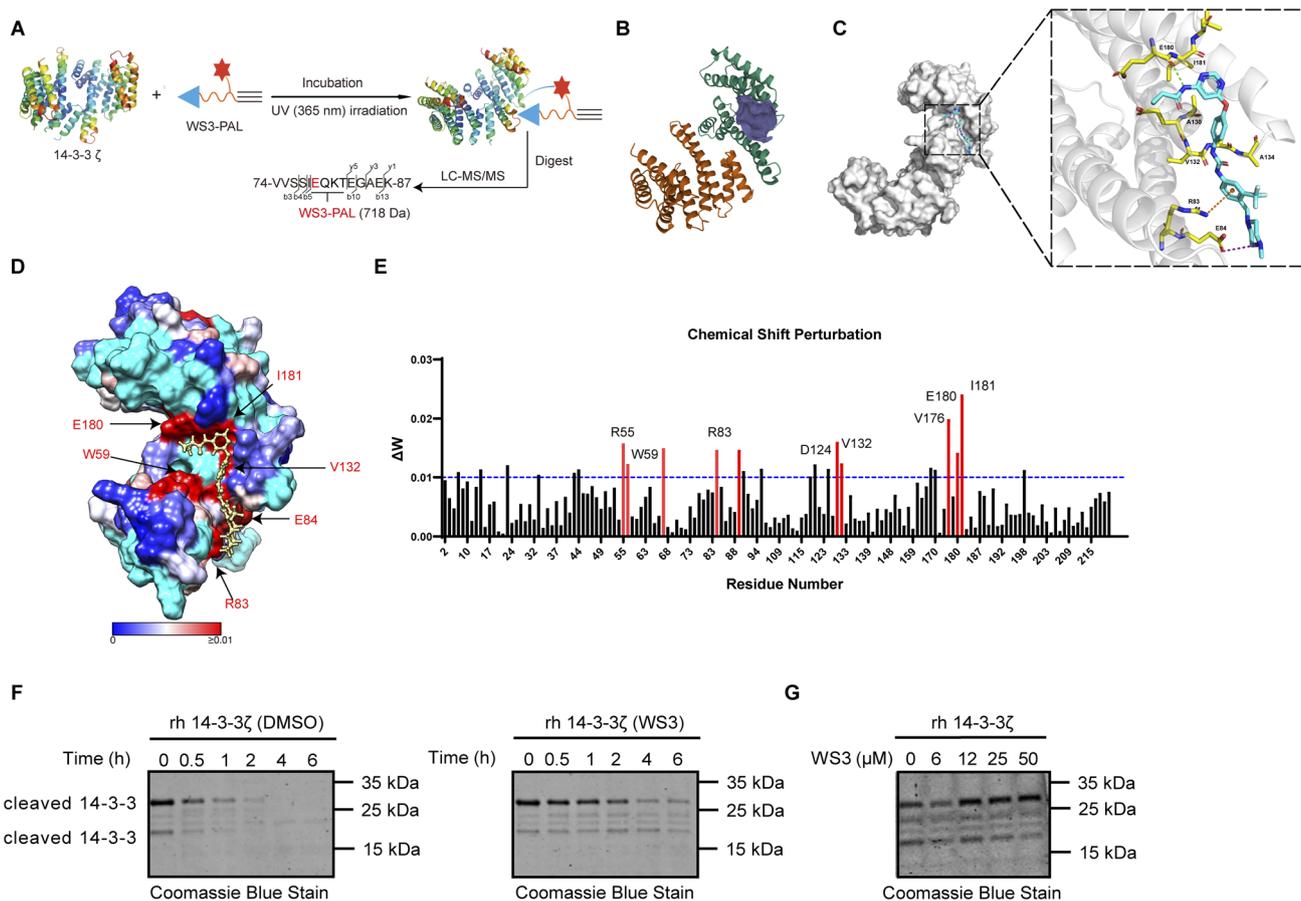
Fig. 3   WS3 binds allosterically to 14-3-3 and drives a conformational change. (A) LC-MS/MS analysis of the WS3-PAL-bound fragment derived from 14-3-3ζ. WS3-PAL was incubated with purified 14-3-3ζ and was then successively subjected to photo-crosslinking, trypsin digestion and MS/MS. The resulting modified peptides were labeled. (B) 14-3-3ζ protein (PDB: 2C1N) allosteric pocket prediction through the online webserver CavityPlus. (C) Predicted molecular docking study of WS3 (cyan) with 14-3-3ζ (PDB: 2C1N, gray). Hydrogen bonds are shown as green dashed lines. The salt bridge is shown as purple dashed lines. Cation–Pi interaction is shown as orange dashed lines. (D) Mapping of residues undergoing chemical shift perturbations onto the surface representation of 14-3-3ζ (PDB: 2C1N). Residues with traceable assigned resonances are colored on a red–white–blue gradient (0 ppm to 0.01 ppm) based on their combined chemical shift [$\Delta\omega = ((\Delta\delta^1H)^2 + (0.2 \times \Delta\delta^{15}N)^2)1/2$]. Unclassified residues are colored cyan. (E) Chemical shift perturbations (CSPs) of ^{15}N-labeled 14-3-3ζ measured in the presence of a 1 : 2 mole ratio of 14-3-3 : WS3 compared to DMSO treated 14-3-3 are plotted as a function of 14-3-3 residue number. Residues with chemical shift perturbations over the threshold are labeled red. (F) Coomassie-stained gels showing limited trypsin (5 nM) digestion of 14-3-3ζ in the presence of WS3 or DMSO (vehicle) carried out for different times at 37 °C. (G) Coomassie-stained gels showing limited trypsin (5 nM) digestion of 14-3-3ζ in the presence of WS3 or DMSO (vehicle) carried out for 1 h at 37 °C. Data are representative of at least 2 biological replicates.

binding groove nor in any previously reported binding pockets, indicating that WS3 binds to an unrecognized allosteric pocket. Next, we utilized the online web tool Cavity Plus[32] to predict the allosteric pocket using the crystal structure of 14-3-3ζ (PDB: 2C1N). The top-ranked pocket based on druggability encompassed the labeled motif, which is a site never targeted by any ligand (Fig. 3B). We then docked WS3 into the potential pocket in 14-3-3ζ (PDB: 2C1N) to generate the preferential binding mode (Fig. 3C). The molecular docking results revealed that WS3 sits in a hydrophobic pocket composed of amino acids W59, A130, V132, A134, I181 and L182. The NH of cyclopropionamide formed a hydrogen bond with the carbonyl group of E180. The pyrimidine ring engaged in hydrophobic interaction with I181, and the benzene ring of WS3 interacts with A130 and V132 via hydrophobic interaction as well. Besides, the trifluoromethyl benzene group formed hydrophobic interaction

with R83 and formed cation–Pi interaction while methylpiperazine formed a salt bridge with E84 and was exposed to solvent. This model agreed well with STD-NMR results. Accordingly, mutating these interactions-involved residues (R83, E84, and E180) to alanine (A) markedly weakened the binding bewteen 14-3-3ζ and WS3-PAL, whereas mutation of the non-interacting residues S63 and E66 had negligible effects (Fig. S4B). Furthermore, direct binding affinity measurements of WS3 with these mutated 14-3-3ζ proteins showed that the mutation of R83, E84 and E180 completely abolished the binding, while mutation of S63 retained the binding (Fig. S4C). Taken together, these results collectively demonstrate that WS3 binds to this atypical allosteric pocket in 14-3-3ζ.

To further elucidate the dynamic interaction between WS3 and 14-3-3ζ, we performed 2D ^1H–^{15}N heteronuclear single quantum coherence (HSQC) NMR analysis using purified ^{15}N
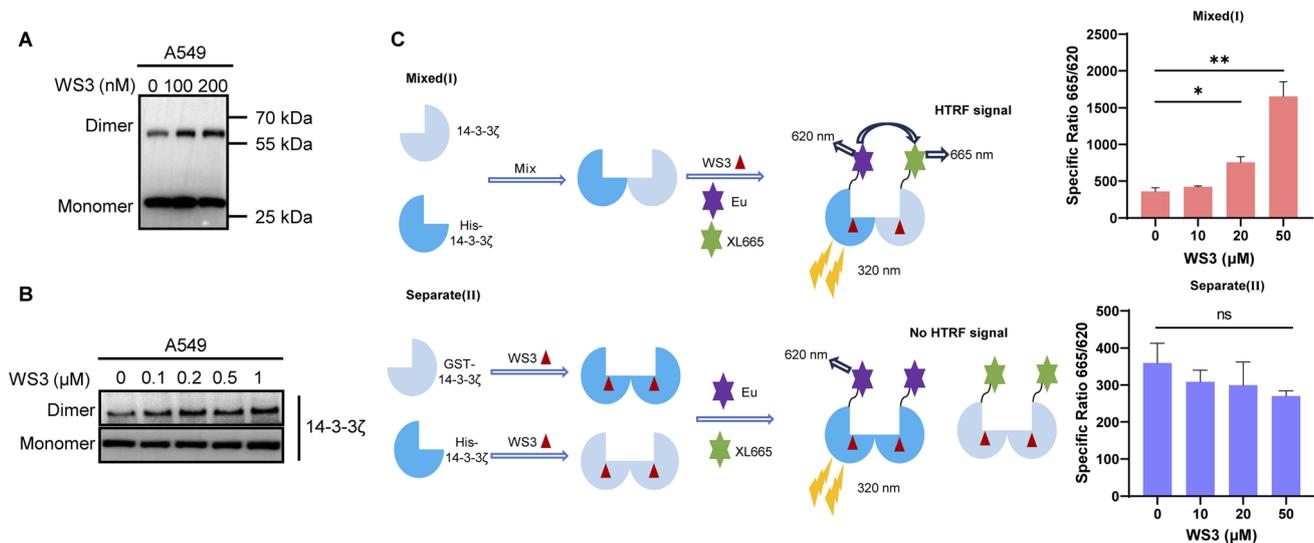
Fig. 4 WS3 stabilizes 14-3-3 dimers both *in vitro* and *in vivo*. (A) Immunoblot analysis of endogenous 14-3-3ζ in A549 cells subjected to WS3 (100 and 200 nM) for 24 h and then treated with crosslinker DSS (1 mM). (B) Immunoblot analysis of the endogenous monomer and dimer form of 14-3-3ζ in A549 cells treated with WS3 (0.1, 0.2, 0.5, and 1 μM) for 12 h by clear native PAGE. (C) HTRF analysis of the dimerization between full-length His-14-3-3 and GST-14-3-3 treated with WS3. Data are representative of at least 2 biological replicates. Statistical analyses are univariate two-sided *t*-tests. **$P < 0.01$.

labeled 14-3-3ζΔC. The previously published sequence-specific backbone assignment of 14-3-3ζΔC was used to analyze changes in 14-3-3ζ backbone amide signals.[33] Addition of WS3 shifted select NMR cross-peaks while preserving the overall features of the NMR spectra. And symmetry is retained upon addition of WS3, which backs up stoichiometry in ITC showing that 1 compound binds to 1 monomer (Fig. S5A). Mapping the chemical shift perturbations (CSPs) on the 14-3-3ζ surface in the presence of WS3 revealed significant shifts in residues located at α4, α5 and α7 of 14-3-3ζ, including W59, R83, E84, A130, E180 and I181 (Fig. 3D, E and Table S3). These residues collectively form a relatively large hydrophobic pocket that aligns well with the predicted WS3 binding site, supporting our simulated binding model of WS3 with 14-3-3ζ. Notably, in addition to the WS3 binding site, several residues within the typical peptide-binding groove also exhibit significant CSPs, including G53, R55, W59, G123, D124, V176, and E180 (Fig. S5B). These findings prompted us to investigate whether WS3 binds to the 14-3-3 dimer and subsequently induces a conformational change that alters the accessibility of the peptide-binding groove, potentially shifting it toward a more open or closed conformation, a mechanism frequently observed in 14-3-3 interactions with its binding partners.[34] To verify our hypothesis, we performed a limited proteolysis assay to assess protein stability upon WS3 treatment. This assay leverages trypsin digestion, which selectively hydrolyzes peptides based on their conformational accessibility, allowing us to evaluate WS3-induced structural changes in 14-3-3. Indeed, WS3 treatment significantly protected purified 14-3-3ζ from digestion by trypsin in a concentration and time dependent manner (Fig. 3F and G), indicating the remarkable conformational change from the apo state to the WS3 bound state.

A previous study demonstrated that 14-3-3ζ dimerization could be dynamically induced *via* an allosteric effect.[35] We, therefore, attempted to determine whether a WS3 induced 14-3-3 conformational change could influence the stabilization of 14-3-3 dimers. We conducted DSS crosslinking assays and found that WS3 enhanced the dimer formation of endogenous 14-3-3ζ in A549 cells, as well as purified 14-3-3ζ (Fig. 4A and S5C). Consistently, the native page analysis indicated that treatment with WS3 resulted in a higher proportion of the 14-3-3ζ dimer than the monomer in A549 cells (Fig. 4B). Furthermore, we performed a homogenous time-resolved FRET assay (HTRF) with His-tagged 14-3-3ζ and GST-tagged 14-3-3ζ to evaluate the 14-3-3ζ dimerization, similar to the previous protocol.[36] As illustrated, the dimer composed of a His-14-3-3ζ and GST-14-3-3ζ could elicit positive HTRF signals. If WS3 stabilizes 14-3-3 dimers, then a pre-incubation of: (i) (GST-14-3-3ζ + WS3) and (His-14-3-3ζ + WS3) separately for 1 h, followed by mixing and addition of HTRF probes, or (ii) (GST-14-3-3ζ + His-14-3-3ζ) for 1 h, followed by mixing and addition of WS3 and HTRF probes, should yield different HTRF signals (Fig. 4C). Consistently, WS3 only further enhanced HTRF signals when pre-incubated with GST-14-3-3ζ and His-14-3-3ζ before addition of WS3. This result supports our hypothesis that WS3 does affect the formation/stabilization of dimers. Collectively, these results imply that WS3 binds to an atypical allosteric site on 14-3-3, altering dimer formation and inducing conformational changes in the protein.

WS3 enhances CUL1–β-TrCP E3 ligase-mediated NRF2 degradation *via* targeted intervention of 14-3-3ζ

To investigate the role of 14-3-3ζ in modulating the NRF2 pathway, we employed both genetic and pharmacological approaches in A549 cells. Knockdown of 14-3-3ζ or

pharmacological inhibition of all 14-3-3 isoforms using the pan-14-3-3 inhibitor difopein[37] both led to reduced NRF2 protein levels (Fig. S6A and S7A) and downregulation of its downstream targets, HO-1 and GCLM (Fig. S6B). Additionally, 14-3-3ζ knockdown accelerated NRF2 turnover in the presence of cycloheximide (CHX) (Fig. S6C), suggesting its role in post-translational regulation. Proteasome inhibition with MG132 rescued NRF2 downregulation caused by 14-3-3ζ knockdown, indicating a proteasome/ubiquitin-dependent degradation mechanism (Fig. S6D and S7B). Immunoblotting further showed that 14-3-3ζ knockdown enhanced NRF2 ubiquitination (Fig. S6E). To determine whether this degradation depends on the SKP1–CUL1–β-TrCP E3 ligase complex, we knocked down CUL1 and β-TrCP. Silencing either component attenuated the effect of 14-3-3ζ knockdown on NRF2 (Fig. S6F and S7C, D).

Given that 14-3-3 proteins could bind and sequester inactive Ser9-phosphorylated GSK3β to suppress GSK3β activity,[38–40] and that GSK3β regulates NRF2 stability by phosphorylating NRF2 at Ser344 to facilitate SKP1–CUL1–β-TrCP E3 ligase-mediated ubiquitination and degradation,[41] we hypothesized that 14-3-3ζ may modulate NRF2 stability through regulation of GSK3β activity. Overexpression of 14-3-3ζ in A549 cells enhanced Ser9-phosphorylation of GSK3β, while its knockdown reduced it (Fig. S6G and H). Co-IP confirmed the interaction between pGSK3β and 14-3-3ζ in A549 cells (Fig. S6H). Moreover, treatment with the GSK3β inhibitor CHIR-99021 partially rescued NRF2 degradation in 14-3-3ζ knockdown cells (Fig. S6I and S7E). Collectively, these results suggest that 14-3-3ζ regulates the CUL1–β-TrCP-mediated NRF2 proteasomal degradation, at least in part, by modulating GSK3β activity.
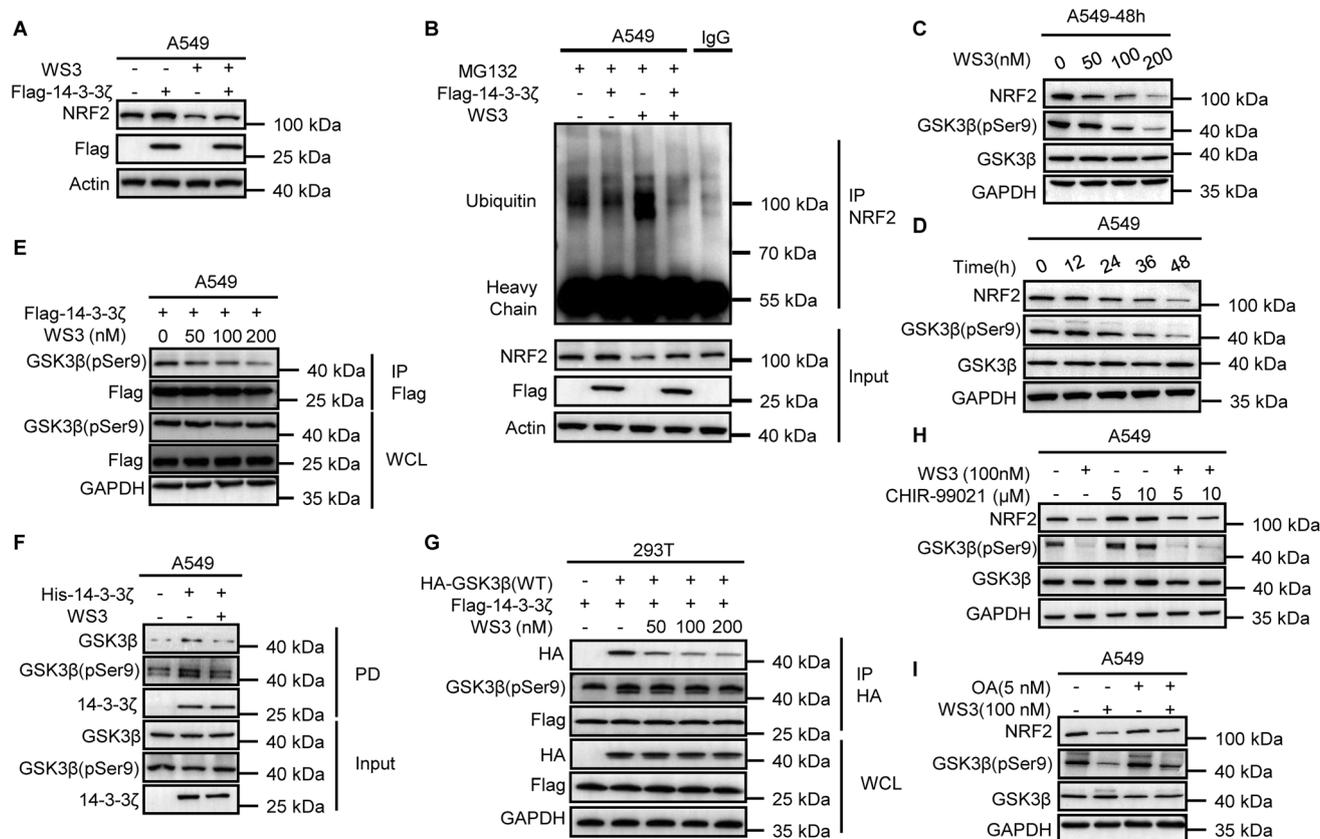

Fig. 5 WS3 promotes NRF2 ubiquitination and degradation through disrupting the interaction between 14-3-3 and pGSK3β. (A) Immunoblot analysis of NRF2 protein in A549 cells. Cells were pre-transfected with the Flag-14-3-3ζ plasmid for 24 h before additional WS3 (200 nM) treatment for 48 h. (B) Immunoblot analysis of NRF2 protein ubiquitination in A549 cells. Cells were pre-transfected with the Flag-14-3-3ζ plasmid for 24 h before additional WS3 (200 nM) treatment for 48 h, and MG132 (10 μM) treatment for 12 h before immunoprecipitation. (C) Immunoblotting analysis of NRF2, pGSK3β and total GSK3β protein in A549 cells. Cells were treated with WS3 (50, 100, and 200 nM) for 48 h. (D) Immunoblotting analysis of NRF2, pGSK3β and total GSK3β protein in A549 cells. Cells were treated with WS3 (200 nM) for the indicated time. (E) A549 cells expressing Flag-14-3-3 were treated with WS3 (50, 100, and 200 nM) or DMSO for 4 h. The whole cell lysates (WCL) from each condition were immunoprecipitated (IP) with anti-Flag beads. WCL and immunoprecipitants were analyzed by immunoblot with the indicated antibodies. (F) His pull-down assays were conducted with His-14-3-3ζ fusion proteins as a bait. Immobilized His-14-3-3ζ proteins were incubated with protein lysate of A549 cells in the presence or absence of WS3 (200 nM) for 12 h. The bound proteins were eluted and subjected to WB analysis. (G) Co-IP analysis of HEK293T cells transiently overexpressing Flag-14-3-3 and HA-GSK3β for 24 h before additional treatment with WS3 (50, 100, and 200 nM) for 12 h. (H) Immunoblot analysis of NRF2, pGSK3β and total GSK3β protein in A549 cells. Cells were pretreated with the GSK3β inhibitor (CHIR-99021 5 μM and 10 μM) for 12 h before additional WS3 (200 nM) treatment for 24 h. (I) Immunoblot analysis of NRF2, pGSK3β and total GSK3β protein in A549 cells. Cells were pretreated with the PP2A inhibitor (OA 5 nM) for 12 h before additional WS3 (200 nM) treatment for 24 h. Data are representative of at least 2 biological replicates.

To determine whether WS3-mediated NRF2 inhibition depends on 14-3-3(ζ), we overexpressed 14-3-3ζ, which significantly reversed WS3-induced NRF2 ubiquitination and degradation (Fig. 5A and B). Similarly, WS3 failed to further reduce NRF2 levels in the presence of the pan-14-3-3 inhibitor difopein (Fig. S7F), indicating that WS3's effect is 14-3-3(ζ)-dependent. A previous study demonstrated that 14-3-3 dimer stabilizers can still disrupt client interactions.[42] Given that WS3 alters dimer formation and induces conformational changes in the binding groove, we examined whether it disrupted the 14-3-3ζ–pGSK3β interaction. WS3 reduced pGSK3β in a time and concentration dependent manner, accompanied by NRF2 downregulation, without affecting total GSK3β (Fig. 5C and D). Short-term WS3 exposure increased NRF2 phosphorylation at Ser344 (Fig. S7G), consistent with active GSK3β signaling. Co-IP in A549 cells expressing Flag-14-3-3ζ showed WS3 concentration dependent reduced pGSK3β association (Fig. 5E), and pull-down assays

using His-14-3-3ζ confirmed reduced pGSK3β binding (Fig. 5F). Similarly, WS3 treatment decreased co-precipitated GSK3β in 293T cells co-transfected with HA-GSK3β and Flag-14-3-3ζ (Fig. 5G). These results suggest that WS3 disrupts the 14-3-3ζ–pGSK3β interaction, relieving GSK3β inhibition to promote NRF2 degradation. Consistently, pretreatment with the GSK3β inhibitor CHIR-99021 partially rescued NRF2 downregulation induced by WS3 (Fig. 5H).

Historically, 14-3-3 binding sequences are generally classified into three canonical motifs – Motif I (RSXpSXP), Motif II (RX(Y/F) XpSXP), and Motif III (pS/TX$_{1-2}$-COOH) – and some non-phosphorylated clients have also been reported.[43] However, GSK3β lacks such a motif, suggesting that it interacts with 14-3-3 in a non-canonical manner. This may provide WS3 with relative selectivity for GSK3β over other 14-3-3 binding partners containing the consensus motif. Consistently, co-IP analysis of A549 cells expressing Flag-14-3-3ζ showed that WS3 did not
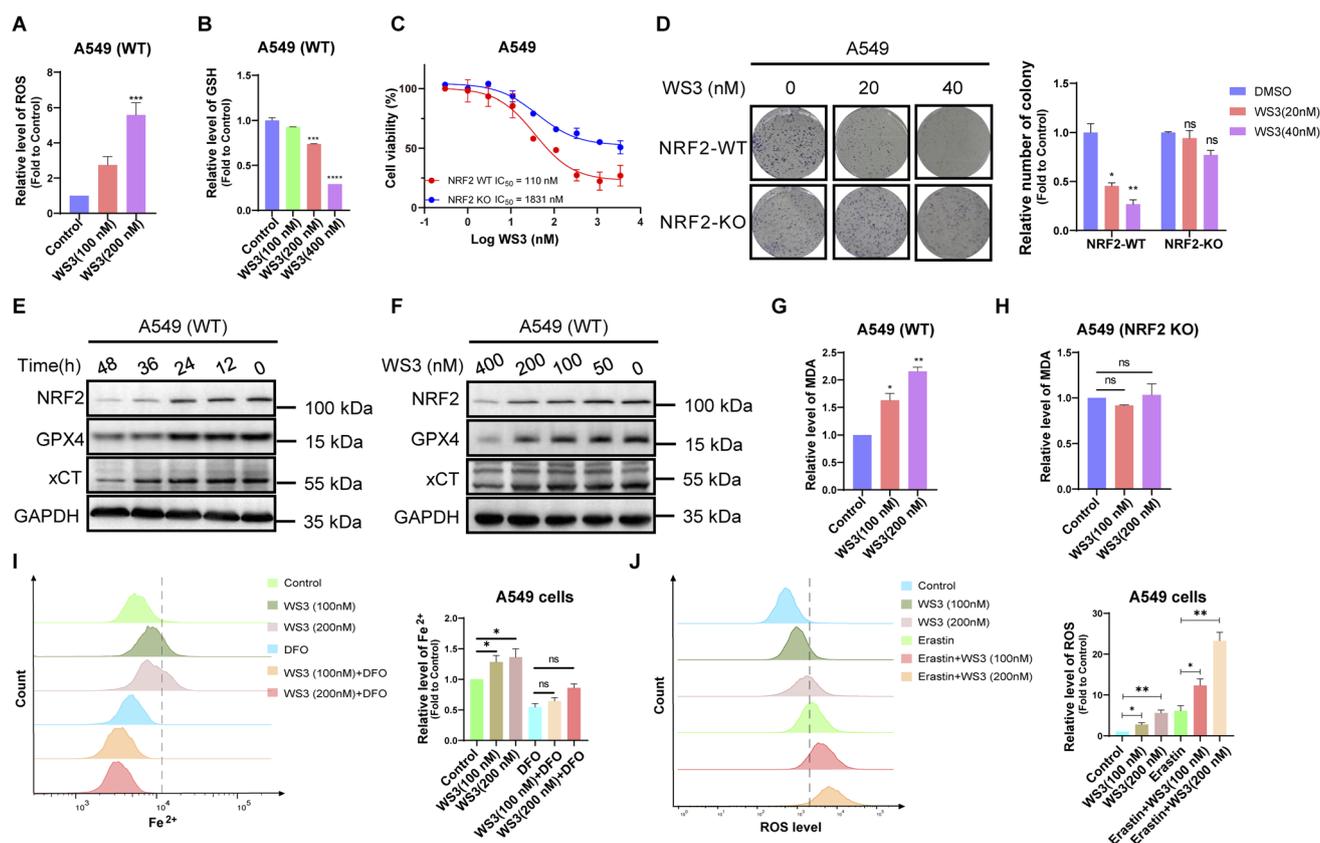

Fig. 6 WS3 induces oxidative stress and ferroptosis and inhibits cell growth in a NRF2 dependent manner. (A) The ROS level in A549 (WT) cells treated with WS3 (100 and 200 nM) for 24 h. The total ROS level was determined using DCFH-DA staining by flow cytometry. Mean and s.e.m. (B) GSH abundance was measured in A549 (WT) cells treated with WS3 (100, 200, and 400 nM) for 24 h. Mean and s.e.m. (C) Cell viability analysis of A549 (WT) or Nrf2-KO cells incubated with WS3 for 48 h. Mean and s.e.m. (D) Quantification and images of A549 (WT) or Nrf2-KO cells colonies formed after 2 week treatment with WS3 (20 or 40 nM) ($n = 3$, mean and s.e.m., univariate two-sided t-test). (E) Immunoblotting analysis GPX4, xCT and NRF2 protein levels in A549 (WT) cells subjected to WS3 (200 nM) treatment for the indicated time. (F) Immunoblotting analysis of GPX4, xCT and NRF2 protein levels in A549 (WT) cells subjected to WS3 (50, 100, 200, and 400 nM) treatment for 36 h. (G) MDA abundance was measured in A549 (WT) cells treated with WS3 (100 and 200 nM) for 24 h. Mean and s.e.m. (H) MDA abundance was measured in A549 (Nrf2 KO) cells treated with WS3 (100 and 200 nM) for 24 h. Mean and s.e.m. (I) A549 cells were treated with 100 and 200 nM WS3 and/or 100 μM DFO for 24 h, and then labeled with FerroOrange to detect the cellular labile iron pool by flow cytometry. DFO was utilized as a positive control to reduce the cellular labile iron pool. Mean and s.e.m. (J) ROS level in A549 cells treated with (100 or 200 nM) WS3 and/or (10 μM) erastin for 24 h. The total ROS level was determined using DCFH-DA staining by flow cytometry. Mean and s.e.m. Statistical analyses are univariate two-sided t-tests. *$P < 0.05$, **$P < 0.01$, ***$P < 0.005$, ***$P < 0.001$, and ****$P < 0.0001$. NS, not significant. Data are representative of at least 2 biological replicates.

affect the interaction between 14-3-3ζ and c-Raf (Motif I), FOXO3A (Motif II) or P27 (Motif III) (Fig. S7H). In contrast, FC-A, a widely used 14-3-3 protein stabilizer that enhances interactions between 14-3-3 and its partners,[44] increased the levels of pGSK3β and NRF2 in A549 cells (Fig. S7I). Moreover, it has been reported that PP2A acts as the main phosphatase that converts inactive pGSK3β into active GSK3β.[45] Thus, we hypothesized that if the NRF2 downregulatory action of WS3 relied on active GSK3β, PP2A inhibitors would rescue it. Indeed, pretreatment with the PP2A inhibitor okadaic acid (OA) partially reversed the NRF2 downregulation caused by WS3 (Fig. 5I). Taken together, these results reveal that WS3 promotes NRF2 degradation by activating GSK3β through disrupting the interaction between pGSK3β and 14-3-3ζ.

WS3 weakens the antioxidant capacity of A549 cells in a NRF2 dependent manner

To evaluate whether WS3 impairs the antioxidant capacity of A549 cells by inhibiting NRF2, we measured reactive oxygen species (ROS) and glutathione (GSH) levels in both A549 cells

and NRF2-KO cells treated with WS3. We found that WS3 induced ROS accumulation and reduced GSH levels in A549 cells in a concentration dependent manner, whereas no such effects were observed in NRF2-KO cells (Fig. 6A, B and S8A, B). This is consistent with the absence of downregulation of NRF2 downstream targets HO-1 and GCLM in NRF2-KO cells (Fig. S8C). In addition to its antioxidant capacity, NRF2 activation is known to contribute to tumor cell growth.[46] In A549 cells, WS3 arrested the cell cycle at the G2/M phase and induced early apoptosis (Fig. S8D and E). Treatment with WS3 significantly inhibited cell proliferation in A549 cells compared to NRF2-KO cells, with an IC_{50} of 110 nM versus 1831 nM (Fig. 6C). Additionally, colony formation assay demonstrated that WS3 markedly reduced the colony numbers formed in A549 cells compared to NRF2-KO cells (Fig. 6D).

Recent studies have established a critical role of NRF2 in suppressing ferroptosis,[47] a type of programmed cell death characterized by the accumulation of lipid peroxides and iron dependency, due to the findings that two major ferroptosis modulators (GPX4 and SLC7A11) are NRF2 target genes.[48,49] As
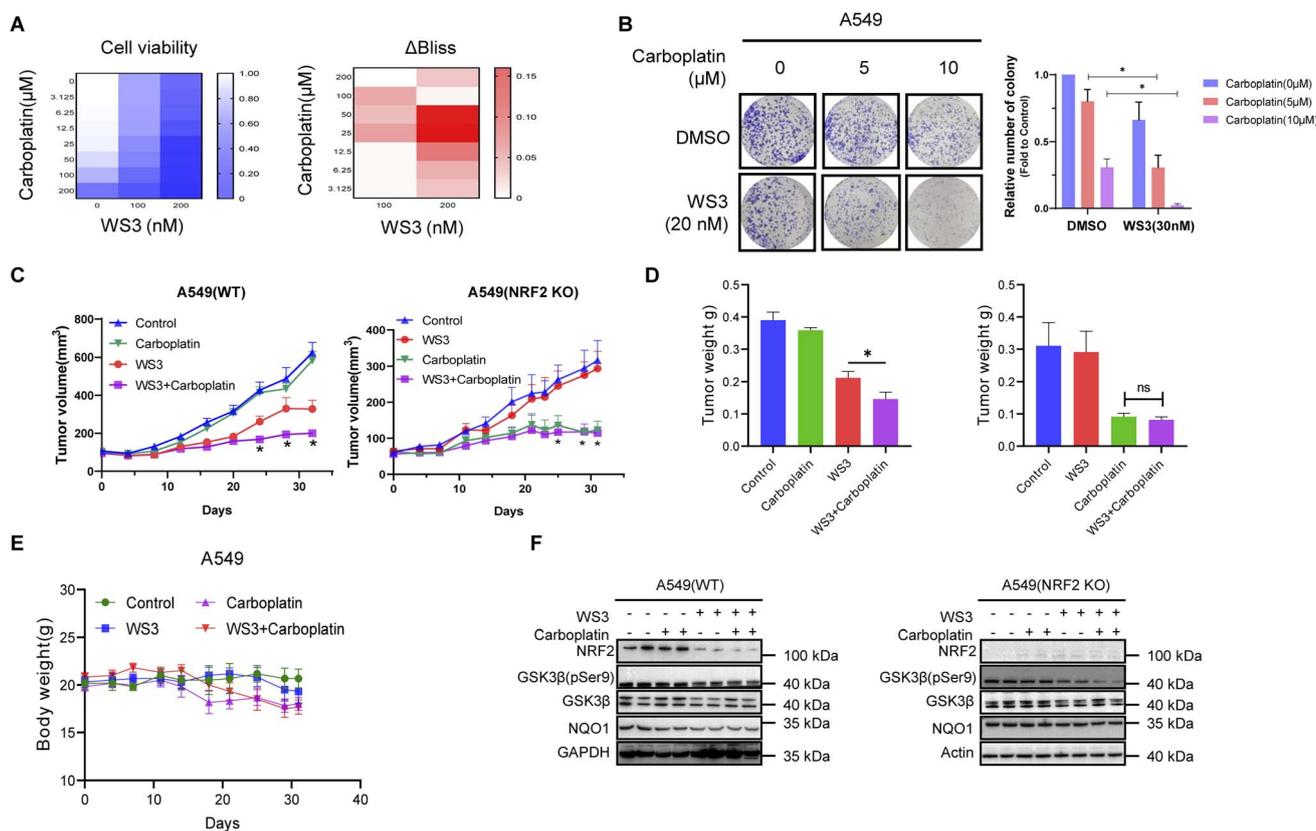

Fig. 7 WS3 showed in vivo efficacy and sensitized the A549 (WT) cell xenograft to carboplatin. (A) Heatmap of cell viability (top) and deviation from Bliss (bottom) in A549 cells following 48 h treatment with WS3 (0, 100, and 200 nM) in combination with a series of carboplatin concentrations (data are representative of 3 biological replicates, mean and s.e.m.). (B) Quantification and images of A549 cell colonies formed after 2 week treatment with WS3 (20 nM) and/or carboplatin (5 or 10 μM) (n = 3, mean and s.e.m., univariate two-sided t-test). (C) Growth curves in tumor volumes of A549 (WT) or Nrf2-KO tumors treated with WS3 (1 mg kg⁻¹) and/or carboplatin (5 mg kg⁻¹) at the indicated dosing schedules (n = 5/group) for 32 days. Variance was estimated separately for each group using weighted least squares, *P < 0.05; ***P < 0.001. (D) Weight of A549 (WT) or NRF2-KO tumors treated with WS3 (1 mg kg⁻¹) and/or carboplatin (5 mg kg⁻¹) at 21 days (data are represented as mean and s.e.m.). (E) Relative body weight changes in mice with A549 tumors. Mice were followed throughout the study. (F) Immunoblotting analysis of NRF2, NQO1 and GSK3β protein levels in A549 (WT) or Nrf2-KO xenograft tumors. 10 mg from each tumor of the same group (n = 2/group) was pooled and subjected to WB analysis.

expected, treatment with WS3 significantly inhibited the expression of GPX4 and SLC7A11 at both the mRNA and protein levels in a concentration and time dependent manner, which is attenuated in NRF2-KO cells (Fig. 6E, F and S8F, G). Additionally, WS3 treatment increased malondialdehyde (MDA) levels, a biomarker of lipid peroxidation, which was also abrogated in NRF2-KO cells (Fig. 6G and H). WS3 increased the level of free Fe^{2+}, as indicated by the enhanced fluorescence intensity of the Fe^{2+}-selective fluorescent probe FerroOrange. Co-treatment with the iron chelator deferoxamine (DFO) reduced the availability of iron and rescued the free Fe^{2+} increase induced by WS3 (Fig. 6I). Moreover, WS3 treatment significantly increased erastin[50] (a ferroptosis inducer)-induced ROS in A549 cells (Fig. 6J). Taken together, these results illustrate that WS3 efficiently dampens antioxidant responses, induces oxidative stress, stimulates ferroptosis and inhibits cell growth in A549 cells, primarily through the inhibition of NRF2.

Inhibiting NRF2 sensitizes A549 cells to chemotherapeutics and ferroptosis

Generally, NRF2 inhibitors are anticipated to sensitize cancer cells to chemotherapy.[51] Cell viability analysis showed that after cotreatment with chemotherapeutic agents, including carboplatin and doxorubicin, WS3 significantly inhibited cell proliferation compared to treatment with either agent alone. Employing the Bliss independence model, we found that the combination of carboplatin and WS3 displayed greater synergy than doxorubicin in A549 cells (Fig. 7A and S9A). Cotreatment of carboplatin and WS3 significantly reduced the colonies formed after two weeks (Fig. 7B). Cell viability analysis showed that cotreatment of WS3 with ferroptosis inducers, including erastin and RSL3, markedly inhibited cell proliferation compared to any single treatment. The Bliss independence model analysis also indicated the synergy effects (Fig. S9B and C).

To investigate the synergistic effects of WS3 and carboplatin on tumor xenografts, we utilized A549 cells and NRF2-KO A549 cells, respectively. While carboplatin alone did not significantly affect A549 tumor growth, WS3 partially inhibited it and the combination of WS3 and carboplatin showed dramatic efficacy (Fig. 7C and S10B, C). In NRF2-KO cell-derived tumors, both carboplatin alone and carboplatin plus WS3 significantly inhibited tumor growth. However, WS3 did not sensitize the NRF2-KO tumors to carboplatin (Fig. 7D), indicating that its synergistic efficacy depends on NRF2. Histological examination of normal tissues and body weight measurement of the WS3 treated mice showed no significant differences from the control (Fig. 7E and S10D), implying that WS3 is well tolerated. Importantly, WS3 did not enhance carboplatin toxicity, as evidenced by similar body weight measurements between the carboplatin and combination treatment groups. WS3 alone or in combination with carboplatin, significantly decreased NRF2 and NQO1 protein levels in A549 tumors but not in NRF2-KO tumors, despite the reduced pGSK3β levels in both groups (Fig. 7F). Meanwhile, WS3 hardly affected NRF2 and NQO1 protein levels in normal lung tissue (Fig. S10E), indicating the selectivity of WS3 in tumor cells. In summary, these results

demonstrate that WS3 is a potent NRF2 inhibitor for chemotherapy against tumors harboring overactivated NRF2 signaling pathways.

Conclusion

Accumulating evidence has firmly established the oncogenic NRF2 signaling pathway in resistance to cancer chemotherapies, targeted therapies and radiotherapies, underscoring the urgent need to develop potent and tumor specific NRF2 inhibitors. Here, we identified WS3 as a potent NRF2 inhibitor through phenotypic screening, which selectively decreased NRF2 protein in tumor cells. To uncover the direct molecular target of WS3, we performed photo-affinity based chemoproteomics and various biophysical assays. We elucidated 14-3-3(ζ) as the main cellular target(s) and demonstrated that allosterically modulating 14-3-3(ζ) by WS3 leads to the enhancement of the functional GSK3β–β-TrCP axis-mediated NRF2 proteasomal degradation. Meanwhile, we demonstrated that WS3 potently weakened the antioxidant capacity of A549 cells in a NRF2 dependent manner, and sensitized cancer cells to chemotherapeutic agents and ferroptosis *in vitro* as well as potentiated chemotherapy efficacy *in vivo*. Given the frequent dysregulation of NRF2 in human cancers, our study uncovers the potential of targeting 14-3-3(ζ) for NRF2-driven cancer treatment.

Similar to NRF2, which is constitutively activated in NSCLC, growing evidence has suggested that overexpressed 14-3-3 protein can promote tumor progression and drug resistance. In this study, we, for the first time, establish a positive correlation between 14-3-3ζ and NRF2 signaling pathways. First, through bioinformatic analysis we identify a positive correlation between the expression of 14-3-3ζ and NRF2 in TCGA-LUAD patients and in NSCLC cell lines (Fig. S11A and B), and find the significant upregulation of several NRF2 signaling pathways in high 14-3-3ζ expression lung cancer. Functional verification illustrates that inhibiting 14-3-3ζ may promote the proteasomal degradation of NRF2 *via* the CUL1–β-TrCP E3 complex. Mechanistically, 14-3-3ζ binds and protects the inactive pGSK3β from dephosphorylation by PP2A, which hinders its ability to phosphorylate NRF2 at Ser344, reducing the CUL1–β-TrCP-mediated NRF2 degradation. Previous study has uncovered that the β-TrCP-mediated pathway indeed cooperates with the Keap1-mediated pathway in the degradation of NRF2 *in vivo*, particularly when the latter is profoundly suppressed.[52] Therefore, in cancers harboring mutations in NFE2L2 or KEAP1, which abolishes the Keap1-mediated pathway, the β-TrCP-mediated pathway becomes critically important. Notably, somatic mutations associated with NRF2 protein accumulation frequently co-occur with mutations related to the activation of the PI3K–AKT signaling pathway in specific cancers.[53] Consequently, GSK3β, a key component of the β-TrCP-mediated pathway, is nearly inactive in those cancers at the basal state due to the enhanced Ser9-phosphorylation caused by the aberrantly activated AKT signaling pathways.[54,55] And our work illustrated that the inactive pGSK3β could be sequestered by 14-3-3 from dephosphorylation by PP2A, thereby hindering its activity in promoting the β-TrCP-mediated NRF2 degradation, further exacerbating the dysregulation of NRF2. Under these

circumstances, we propose that reshaping the 14-3-3 hub to boost the GSK3β activity may hold great potential. Nevertheless, due to the lack of structural information on the 14-3-3–pGSK3β complex, the precise molecular mechanism by which WS3 disrupts their interaction remains incompletely defined. Future crystallographic studies will be required to elucidate this in detail. Furthermore, as our cellular assays were primarily conducted in A549 cells, the efficacy of WS3 in other contexts of NRF2 hyperactivation is yet to be determined. Additional studies are warranted to assess the therapeutic potential of WS3 in a broader range of NRF2-driven cancers.

While most reported small molecules primarily bind in or around the central groove of 14-3-3 proteins to stabilize or inhibit the 14-3-3-substrate interaction,[56–60] WS3 binds in an atypical allosteric pocket with nanomole to sub-micromole affinity for the 14-3-3 proteins. Notably, this interaction alters the stabilization of 14-3-3 dimers and drives a conformational change in the peptide-binding groove. Our study demonstrates that WS3 could interrupt the interaction between 14-3-3 and pGSK3β, leading to the dephosphorylation of GSK3β at Ser9 and its subsequent activation. Activated GSK3β facilitates the phosphorylation of NRF2 at Ser344, resulting in the CUL1–β-TrCP E3 ligase dependent NRF2 degradation. However, as WS3 binds to multiple 14-3-3 isoforms, it may act as a pan-14-3-3 inhibitor. Proteomics-based studies are still needed to evaluate potential off-target interactions and broader changes in the interactome following WS3 treatment. A future objective will be to develop inhibitors with defined subtype selectivity.

Interestingly, WS3 exhibited nanomolar potency in cellular assays, in contrast to its micromolar affinity observed in biophysical assays. One plausible explanation is a pathway amplification effect. Mechanistically, WS3 allosterically perturbs the 14-3-3ζ–pGSK3β interaction, thereby restoring GSK3β activity. Even partial reactivation of GSK3β is sufficient to phosphorylate NRF2, marking it for β-TrCP-mediated ubiquitination and proteasomal degradation. Given that NRF2 controls a broad transcriptional program of antioxidant and cytoprotective genes, its stability is embedded within a nonlinear regulatory circuit. This feed-forward architecture may therefore amplify the phenotypic response to WS3, accounting for the observed discrepancy.

In summary, our work establishes an unrecognized role of 14-3-3 in the dysregulation of NRF2 in NSCLC by restricting GSK3β activity, which is crucial for mediating NRF2 proteasomal degradation. Meanwhile, we propose a novel strategy for repressing NRF2-driven cancers through allosterically modulating 14-3-3(ζ) to promote NRF2 degradation. Additionally, we introduce WS3 as a first-in-class sub-micromolar 14-3-3 modulator with a distinct binding mode, laying the foundation for the development of more potent and selective chemical tools to further investigate the biological roles of 14-3-3 proteins in cancer and other diseases.

Ethical statement

All animal experiments were approved by local ethical review and were carried out in accordance with federal and institutional guidelines under a protocol approved by the Institutional Animal Care and Use Committee at China Pharmaceutical University.

Author contributions

T. L. performed the phenotypic screening. J. Z. synthesized and purified the compounds with help from H. J. J. Z. performed most of the cellular assays with help from T. L. and K. Z. J. Z., Q. Z., Z. Z. and J. W. performed *in vivo* experiments. J. Z. wrote the manuscript with input from all authors. Q. Y., M. L. and Z. J. provided supervision. All authors discussed the results and commented on the manuscript.

Conflicts of interest

The authors declare no conflict of interest.

Data availability

The data supporting this article have been included as part of the SI. It includes supplementary figures and tables; chemical experimental section; bioactivity experimental procedures; NMR spectra, HPLC report and HR-MS report of synthesized compounds; uncropped gels or blots. See DOI: **https://doi.org/10.1039/d5sc04324g**.

Acknowledgements

References

1 M. Rojo de la Vega, E. Chapman and D. D. Zhang, *Cancer Cell*, 2018, **34**, 21–43.

2 G. M. DeNicola, F. A. Karreth, T. J. Humpton, A. Gopinathan, C. Wei, K. Frese, D. Mangal, K. H. Yu, C. J. Yeo, E. S. Calhoun, F. Scrimieri, J. M. Winter, R. H. Hruban, C. Iacobuzio-Donahue, S. E. Kern, I. A. Blair and D. A. Tuveson, *Nature*, 2011, **475**, 106–109.

3 A. Cuadrado, A. I. Rojo, G. Wells, J. D. Hayes, S. P. Cousin, W. L. Rumsey, O. C. Attucks, S. Franklin, A. L. Levonen, T. W. Kensler and A. T. Dinkova-Kostova, *Nat. Rev. Drug Discovery*, 2019, **18**, 295–317.

4 T. Weiss-Sadan, M. Ge, M. Hayashi, M. Gohar, C.-H. Yao, A. de Groot, S. Harry, A. Carlin, H. Fischer, L. Shi, T.-Y. Wei, C. H. Adelmann, K. Wolf, T. Vornbäumen, B. R. Dürr, M. Takahashi, M. Richter, J. Zhang, T.-Y. Yang, V. Vijay, D. E. Fisher, A. N. Hata, M. C. Haigis, R. Mostoslavsky, N. Bardeesy, T. Papagiannakopoulos and L. Bar-Peled, *Cell Metab.*, 2023, **35**, 487–503.

5 J. D. Hayes, A. T. Dinkova-Kostova and K. D. Tew, *Cancer Cell*, 2020, **38**, 167–197.

6 A. Loboda, M. Damulewicz, E. Pyza, A. Jozkowicz and J. Dulak, *Cell. Mol. Life Sci.*, 2016, **73**, 3221–3247.

7 Z. Y. Jiang, M. C. Lu and Q. D. You, *J. Med. Chem.*, 2019, **62**, 3840–3856.

8 D. Ren, N. F. Villeneuve, T. Jiang, T. Wu, A. Lau, H. A. Toppin and D. D. Zhang, *Proc. Natl. Acad. Sci. U. S. A.*, 2011, **108**, 1433–1438.

9 A. Singh, S. Venkannagari, K. H. Oh, Y. Q. Zhang, J. M. Rohde, L. Liu, S. Nimmagadda, K. Sudini, K. R. Brimacombe, S. Gajghate, J. Ma, A. Wang, X. Xu, S. A. Shahane, M. Xia, J. Woo, G. A. Mensah, Z. Wang, M. Ferrer, E. Gabrielson, Z. Li, F. Rastinejad, M. Shen, M. B. Boxer and S. Biswal, *ACS Chem. Biol.*, 2016, **11**, 3214–3225.

10 D. Zhang, Z. Hou, K. E. Aldrich, L. Lockwood, A. L. Odom and K. T. Liby, *Mol. Cancer Ther.*, 2021, **20**, 1692–1701.

11 T. Aboulkassim, X. Tian, Q. Liu, D. Qiu, M. Hancock, J. H. Wu and G. Batist, *Cell Rep.*, 2023, **42**, 113104.

12 N. Roy, T. Wyseure, I. C. Lo, J. Metzger, C. L. Eissler, S. M. Bernard, I. Bok, A. N. Snead, A. Parker, J. C. Green, J. Inloes, S. R. Jacinto, B. Kuenzi, B. D. Horning, N. Ibrahim, S. Grabow, H. Panda, D. P. Bhatt, P. Zolkind, Z. Rush, K. Negri, H. N. Williams, E. Walton, M. K. Pastuszka, J. J. Sigler, E. Tran, K. Hee, J. McLaughlin, G. Ambrus-Aikelin, J. Pollock, R. T. Abraham, T. M. Kinsella, G. M. Simon, M. B. Major, D. S. Weinstein and M. P. Patricelli, *bioRxiv*, 2024, preprint, DOI: [10.1101/2024.10.04.616592](10.1101/2024.10.04.616592).

13 D. D. Zhang, *Nat. Rev. Drug Discovery*, 2025, **24**, 421–444.

14 J. D. Hayes and A. T. Dinkova-Kostova, *Trends Biochem. Sci.*, 2014, **39**, 199–218.

15 C. Tonelli, I. I. C. Chio and D. A. Tuveson, *Antioxid. Redox Signaling*, 2018, **29**, 1727–1745.

16 M. Yamamoto, T. W. Kensler and H. Motohashi, *Physiol. Rev.*, 2018, **98**, 1169–1203.

17 T. Suzuki, J. Takahashi and M. Yamamoto, *Mol. Cells*, 2023, **46**, 133–141.

18 P. Cohen and M. Goedert, *Nat. Rev. Drug Discovery*, 2004, **3**, 479–487.

19 L. M. Stevers, E. Sijbesma, M. Botta, C. MacKintosh, T. Obsil, I. Landrieu, Y. Cau, A. J. Wilson, A. Karawajczyk, J. Eickhoff, J. Davis, M. Hann, G. O'Mahony, R. G. Doveston, L. Brunsveld and C. Ottmann, *J. Med. Chem.*, 2018, **61**, 3755–3778.

20 H. Hermeking, *Nat. Rev. Cancer*, 2003, **3**, 931–943.

21 X. Yang, W. H. Lee, F. Sobott, E. Papagrigoriou, C. V. Robinson, J. G. Grossmann, M. Sundstrom, D. A. Doyle and J. M. Elkins, *Proc. Natl. Acad. Sci. U. S. A.*, 2006, **103**, 17237–17242.

22 Y. Aghazadeh and V. Papadopoulos, *Drug Discovery Today*, 2016, **21**, 278–287.

23 E. Park, S. Rawson, K. Li, B. W. Kim, S. B. Ficarro, G. G. Pino, H. Sharif, J. A. Marto, H. Jeon and M. J. Eck, *Nature*, 2019, **575**, 545–550.

24 J. Shen, F. Jiang, Y. Yang, G. Huang, F. Pu, Q. Liu, L. Chen, L. Ju, M. Lu, F. Zhou, C. Zhang, X. Luo, X. Yang, C. Jiao, X. Li, Z. Li, Y. Li and J. Zhang, *J. Hepatol.*, 2016, **65**, 953–962.

25 S. Liu, R. Guo, H. Xu, J. Yang, H. Luo, S. J. Yeung, K. Li, M. H. Lee and R. Yang, *Cell Rep.*, 2023, **42**, 112870.

26 Y. Gan, F. Ye and X. X. He, *J. Cancer*, 2020, **11**, 2252–2264.

27 S. Scalera, M. Mazzotta, C. Cortile, E. Krasniqi, R. De Maria, F. Cappuzzo, G. Ciliberto and M. Maugeri-Saccà, *J. Thorac. Oncol.*, 2022, **17**, 751–757.

28 W. Shen, M. S. Tremblay, V. A. Deshmukh, W. Wang, C. M. Filippi, G. Harb, Y. Q. Zhang, A. Kamireddy, J. E. Baaten, Q. Jin, T. Wu, J. G. Swoboda, C. Y. Cho, J. Li, B. A. Laffitte, P. McNamara, R. Glynne, X. Wu, A. E. Herman and P. G. Schultz, *J. Am. Chem. Soc.*, 2013, **135**, 1669–1672.

29 U. Rix and G. Superti-Furga, *Nat. Chem. Biol.*, 2009, **5**, 616–624.

30 Z. Trosanova, P. Lousa, A. Kozelekova, T. Brom, N. Gasparik, J. Tungli, V. Weisova, E. Zupa, G. Zoldak and J. Hritz, *J. Mol. Biol.*, 2022, **434**, 167479.

31 N. N. Sluchanko, *Adv. Protein Chem. Struct. Biol.*, 2022, **130**, 289–324.

32 S. Wang, J. Xie, J. Pei and L. Lai, *J. Mol. Biol.*, 2023, **435**, 168141.

33 R. C. Killoran, J. Fan, D. Yang, B. H. Shilton and W. Y. Choy, *PLoS One*, 2015, **10**, e0123934.

34 B. Andlovic, D. Valenti, F. Centorrino, F. Picarazzi, S. Hristeva, M. Hiltmann, A. Wolf, F. X. Cantrelle, M. Mori, I. Landrieu, L. M. Levy, B. Klebl, D. Tzalis, T. Genski, J. Eickhoff and C. Ottmann, *Biochemistry*, 2024, **63**, 2196–2206.

35 H. Yuan, K. Michelsen and B. Schwappach, *Curr. Biol.*, 2003, **13**, 638–646.

36 H. J. Brink, R. Riemens, S. Thee, B. Beishuizen, D. da Costa Pereira, M. Wijtmans, I. de Esch, M. J. Smit and A. H. de Boer, *ChemBioChem*, 2022, **23**, e202200178.

37 S. C. Masters and H. Fu, *J. Biol. Chem.*, 2001, **276**, 45193–45200.

38 G. Gogl, K. V. Tugaeva, P. Eberling, C. Kostmann, G. Trave and N. N. Sluchanko, *Nat. Commun.*, 2021, **12**, 1677.

39 T. Li and H. K. Paudel, *Neurosci. Lett.*, 2007, **414**, 203–208.

40 J. Zhen, K. Jiao, K. Yang, M. Wu, Q. Zhou, B. Yang, W. Xiao, C. Hu, M. Zhou and Z. Li, *Cell Biol. Toxicol.*, 2021, **37**, 515–529.

41 T. Liu, Y. F. Lv, J. L. Zhao, Q. D. You and Z. Y. Jiang, *Free Radical Biol. Med.*, 2021, **168**, 129–141.

42 Y. J. Wan, L. X. Liao, Y. Liu, H. Yang, X. M. Song, L. C. Wang, X. W. Zhang, Y. Qian, D. Liu, X. M. Shi, L. W. Han, Q. Xia, K. C. Liu, Z. Y. Du, Y. Jiang, M. B. Zhao, K. W. Zeng and P. F. Tu, *Theranostics*, 2020, **10**, 797–815.

43 K. Rittinger, J. Budman, J. A. Xu, S. Volinia, L. C. Cantley, S. J. Smerdon, S. J. Gamblin and M. B. Yaffe, *Mol. Cell*, 1999, **4**, 153–166.

44 R. Rose, S. Erdmann, S. Bovens, A. Wolf, M. Rose, S. Hennig, H. Waldmann and C. Ottmann, *Angew. Chem., Int. Ed.*, 2010, **49**, 4129–4132.

45 D. Chu, J. Tan, S. Xie, N. Jin, X. Yin, C. X. Gong, K. Iqbal and F. Liu, *J. Alzheimer's Dis.*, 2016, **49**, 365–375.

46 Y. Mitsuishi, H. Motohashi and M. Yamamoto, *Front. Oncol.*, 2012, **2**, 200.

47 A. Anandhan, M. Dodson, C. J. Schmidlin, P. Liu and D. D. Zhang, *Cell Chem. Biol.*, 2020, **27**, 436–447.

48 S. J. Dixon, K. M. Lemberg, M. R. Lamprecht, R. Skouta, E. M. Zaitsev, C. E. Gleason, D. N. Patel, A. J. Bauer, A. M. Cantley, W. S. Yang, B. Morrison 3rd and B. R. Stockwell, *Cell*, 2012, **149**, 1060–1072.

49 B. Hassannia, P. Vandenabeele and T. Vanden Berghe, *Cancer Cell*, 2019, **35**, 830–849.

50 Y. Zhang, H. Tan, J. D. Daniels, F. Zandkarimi, H. Liu, L. M. Brown, K. Uchida, O. A. O'Connor and B. R. Stockwell, *Cell Chem. Biol.*, 2019, **26**, 623–633.

51 R. Srivastava, R. Fernandez-Gines, J. A. Encinar, A. Cuadrado and G. Wells, *Free Radical Biol. Med.*, 2022, **192**, 246–260.

52 A. Kuga, K. Tsuchida, H. Panda, M. Horiuchi, A. Otsuki, K. Taguchi, F. Katsuoka, M. Suzuki and M. Yamamoto, *Mol. Cell. Biol.*, 2022, **42**, e0056321.

53 F. Sanchez-Vega, M. Mina, J. Armenia, W. K. Chatila, A. Luna, K. C. La, S. Dimitriadoy, D. L. Liu, H. S. Kantheti, S. Saghafinia, D. Chakravarty, F. Daian, Q. Gao, M. H. Bailey, W. W. Liang, S. M. Foltz, I. Shmulevich, L. Ding, Z. Heins, A. Ochoa, B. Gross, J. Gao, H. Zhang, R. Kundra, C. Kandoth, I. Bahceci, L. Dervishi, U. Dogrusoz, W. Zhou, H. Shen, P. W. Laird, G. P. Way, C. S. Greene, H. Liang, Y. Xiao, C. Wang, A. Iavarone, A. H. Berger, T. G. Bivona, A. J. Lazar, G. D. Hammer, T. Giordano, L. N. Kwong, G. McArthur, C. Huang, A. D. Tward, M. J. Frederick, F. McCormick, M. Meyerson, Cancer Genome Atlas Research Network, E. M. Van Allen, A. D. Cherniack, G. Ciriello, C. Sander and N. Schultz, *Cell*, 2018, **173**, 321–337.

54 K. M. Cahuzac, A. Lubin, K. Bosch, N. Stokes, S. M. Shoenfeld, R. Zhou, H. Lemon, J. Asara and R. E. Parsons, *Cell Rep.*, 2023, **42**, 112536.

55 M. Elgendy, M. Cirò, A. Hosseini, J. Weiszmann, L. Mazzarella, E. Ferrari, R. Cazzoli, G. Curigliano, A. DeCensi, B. Bonanni, A. Budillon, P. G. Pelicci, V. Janssens, M. Ogris, M. Baccarini, L. Lanfrancone, W. Weckwerth, M. Foiani and S. Minucci, *Cancer Cell*, 2019, **35**, 798–815.

56 M. Ehlers, J. N. Grad, S. Mittal, D. Bier, M. Mertel, L. Ohl, M. Bartel, J. Briels, M. Heimann, C. Ottmann, E. Sanchez-Garcia, D. Hoffmann and C. Schmuck, *ChemBioChem*, 2018, **19**, 591–595.

57 H. Wu, J. Ge and S. Q. Yao, *Angew. Chem., Int. Ed.*, 2010, **49**, 6528–6532.

58 J. Zhao, Y. Du, J. R. Horton, A. K. Upadhyay, B. Lou, Y. Bai, X. Zhang, L. Du, M. Li, B. Wang, L. Zhang, J. T. Barbieri, F. R. Khuri, X. Cheng and H. Fu, *Proc. Natl. Acad. Sci. U. S. A.*, 2011, **108**, 16212–16216.

59 M. Mori, G. Vignaroli, Y. Cau, J. Dinic, R. Hill, M. Rossi, D. Colecchia, M. Pesic, W. Link, M. Chiariello, C. Ottmann and M. Botta, *ChemMedChem*, 2014, **9**, 973–983.

60 Z. Gao, T. Fan, L. Chen, M. Yang, V. K. Wai Wong, D. Chen, Z. Liu, Y. Zhou, W. Wu, Z. Qiu, C. Zhang, Y. Li and Y. Jiang, *Eur. J. Med. Chem.*, 2022, **238**, 114402.